Improving the Performance of Brushless DC Motor Using the Six Digits form of SVPWM Switching Mode

A. Alshehabi, M. H. Ferdowsi, and M. R. Alizadeh Pahlavani

Malek-Ashtar University of Technology (MUT), Tehran, Iran

ABSTRACT

In this paper the successful application of Space Vector Pulse Width Modulation (SVPWM) using six digits switching mode applied to Brushless DC motor (BLDC) drive with a view to reduce torque ripple is proposed. The current ripple, created due to the stator winding inductance, leads to generation of ripple in the torque and prevents the usage of BLDC motor in a precise servo drive system. SVPWM techniques enjoy an assortment of advantages such as high output quality, less THD, low distortion and low rating of filter component. Also a current controlled technique for BLDC motor drives is used. The paper includes MATLAB/SIMULINK results of SVPWM three and six digits switching modes. The comparison of simulation results reveals that the SVPWM six digits technique is effective in reducing the ripple. This control method improves the system performance with low torque ripple thus making it suitable for immense applications employing electromechanical actuators.

KEYWORDS: Current Controlled SVPWM, BLDC Motor, Six Digits Switching, Minimization of Torque Ripple, THD

1. INTRODUCTION

In the past few years the field of controlled electrical drives has undergone rapid expansion due to the technological improvements in semiconductor devices. New electronic microprocessors and DSPs which provide amazing computational speeds have enabled the development of effective vector controlled AC drives with lower power dissipation and more accurate control. Brushless Direct Current (BLDC) motors are one of the motor types rapidly gaining popularity. BLDC motors are used in industries such as Appliances, Automotive, Aerospace, Consumer, Medical, Industrial Automation Equipment and Instrumentation. As the name implies, BLDC motors do not use brushes for commutation; instead, they are electronically commutated. BLDC motors have many advantages over brushed DC motors and induction motors [1-6]. A few of these are:

1. Better speed versus torque characteristics
2. High dynamic response
3. Higher speed ranges
4. Long operating life
5. High efficiency
6. Noiseless operation

In addition, the ratio of torque delivered to the size of the motor is higher, making it useful in applications where space and weight are critical factors. This terminology 'Brushless dc motor' is becoming accepted for a self synchronous machine in which the air gap flux distribution and counter EMF, or back-EMF, waveform are approximately trapezoidal as in conventional dc machine. Standard synchronous machine require sinusoidal current excitation, whereas the trapezoidal machine is energized with square-wave or quasi square-wave excitation. The cross-sectional view of a BLDC motor is as shown in Fig.1.
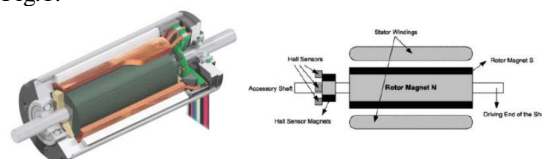

Fig.1. Brushless DC motor cross-sectional view.

However, in a practical BLDC drive, since machine has both inductance and resistance, the stator currents are different from the ideal case and the currents reach to their final values with delay. In other words, circuit has a time constant. Therefore, the current ripple is produced by influence of the inductance and the torque ripple is affected by current ripple directly [7]. The torque ripple

*Corresponding Author: A. Alshehabi, Malek-Ashtar University of Technology (MUT), Tehran, Iran.
Email: amer.shehabi@hotmail.com

generated in commutation period is the main drawback of BLDC motor which deteriorates the precision of BLDC motor [8], [9].Therefore, the torque ripple minimization or elimination is a considerable issue in BLDC motor drives. Several theoretical approaches for analysis of the commutation torque ripple have been reported in literature [10], [11]. A direct torque control (DTC) by employing a hybrid 2- phase and 3-phase switching mode during the commutation periods was presented in [12]. Commutation torque ripple reduction was reported in [13] which based on a fact that current slopes of the incoming and outgoing phases during the commutation interval can be equalized by a proper duty-ratio control. Adaptive torque ripple control for current shaping during commutation was proposed in [14]. A current control method has been presented in [15] to reduce torque ripple. In this paper, a current controlled Space Vector PWM technique for torque ripple reduction is proposed using the three and six digits switching mode [16], [17], [18], [19].

2. BLDC Motor Operation Principle

Permanent magnet DC motors use mechanical commutator and brushes to achieve the commutation. However, BLDC motors adopt Hall Effect sensors in place of mechanical commutator and brushes. The stators of BLDC motors are the coils, and the rotors are the permanent magnets. The stators develop the magnetic fields to make the rotor rotating. Hall-Effect sensors detect the rotor position as the commutating signals. Therefore, the BLDC motors use permanent magnets instead of coils in the armature and so do not need brushes. In this paper, a three-phase and two-pole BLDC motor is used. For the three phases BLDC motor the back-EMF and current waveforms with $120°$ conduction mode are shown in Fig. 2.
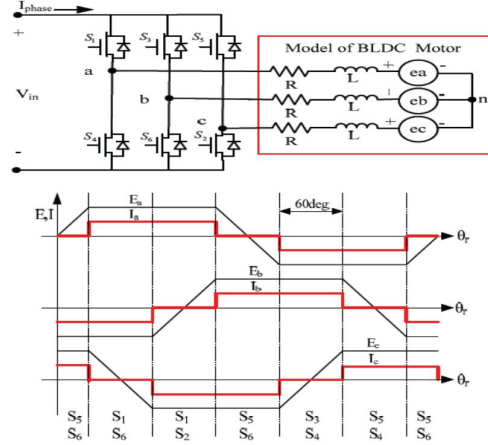

Fig. 2. Configuration of BLDC motor drive system, back-EMF pattern and reference current generation

The analysis of a BLDC motor is represented in [20] as the following equations:

$$\begin{bmatrix} v_a \\ v_b \\ v_c \end{bmatrix} = \begin{bmatrix} R & 0 & 0 \\ 0 & R & 0 \\ 0 & 0 & R \end{bmatrix} \begin{bmatrix} i_a \\ i_b \\ i_c \end{bmatrix}$$
$$+ \begin{bmatrix} L-M & 0 & 0 \\ 0 & L-M & 0 \\ 0 & 0 & L-M \end{bmatrix} \frac{d}{dt} \begin{bmatrix} i_a \\ i_b \\ i_c \end{bmatrix} + \begin{bmatrix} e_a \\ e_b \\ e_c \end{bmatrix} \qquad (1)$$

where v_a, v_b, v_c are the phase voltages, i_a, i_b, i_c are the phase currents, e_a, e_b, e_c are the phase back-k-EMF waveforms, R is the phase resistance, L is the self inductance of each phase and M is the mutual inductance between any two phases. So the electromagnetic torque can be obtained as:

$$T_e = \frac{1}{\omega_r} (e_a i_a + e_b i_b + e_c i_c) \qquad (2)$$

where ω_r is the mechanical speed of the rotor and T_e is the electromagnetic torque. The equation of motion is:

$$\frac{d}{dt} \omega_r = \frac{1}{J} (T_e - T_L - B\omega_r) \qquad (3)$$

B is the damping constant, J is the moment of inertia of the drive and T_L is the load torque. The electrical frequency related to the mechanical speed for a motor with P number of pole pairs:

$$\omega_e = P\,\omega_r \qquad\qquad (4)$$

The instantaneous induced EMFs can be written as given in equation:

$$e_a = f_a(\theta_r)\lambda_p\,\omega_m$$
$$e_b = f_b(\theta_r)\lambda_p\,\omega_m \qquad\qquad (5)$$
$$e_c = f_c(\theta_r)\lambda_p\,\omega_m$$

Where, ω_m is the rotor mechanical speed and θ_r is the rotor electrical position. The state variable (θ_r), rotor position, is required to have the function $f_a(\theta_r)$, which is given as the trapezoidal function (Eq.(6)-(8)). The induced EMFs do not have sharp corners, as is shown in trapezoidal functions. The EMFs are the result of the flux linkages derivatives, and the flux linkages are continuous functions. Fringing also makes the flux density functions smooth with no abrupt edges. Fig.3 shows the application of EMFs generator in Matlab.

$$f_a(\theta_r) = \begin{cases} 1 & 0 < \theta_r < \pi/3 \\ (\dfrac{\pi}{2} - \theta_r)\dfrac{6}{\pi} & \pi/3 < \theta_r < 2\pi/3 \\ -1 & 2\pi/3 < \theta_r < \pi \\ -1 & \pi < \theta_r < 4\pi/3 \\ (\theta_r - \dfrac{3\pi}{2})\dfrac{6}{\pi} & 4\pi/3 < \theta_r < 5\pi/3 \\ 1 & 5\pi/3 < \theta_r < 2\pi \end{cases} \qquad (6)$$

Similarly

$$f_b(\theta_r) = f_a(\theta_r + \frac{2\pi}{3}) \qquad\qquad (7)$$

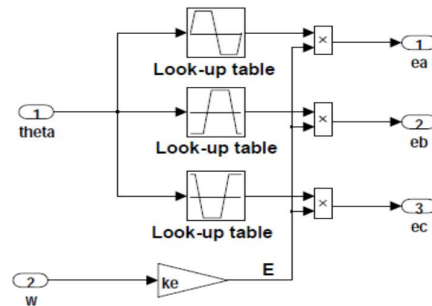$$f_c(\theta_r) = f_a(\theta_r - \frac{2\pi}{3}) \qquad\qquad (8)$$

Fig.3 Block diagram of EMFs generator.

3. Model of BLDC Motor Drive System

The BLDC motor drive system is developed using MATLAB/Simulink. Fig.4 shows the block diagram of BLDC motor drive system.
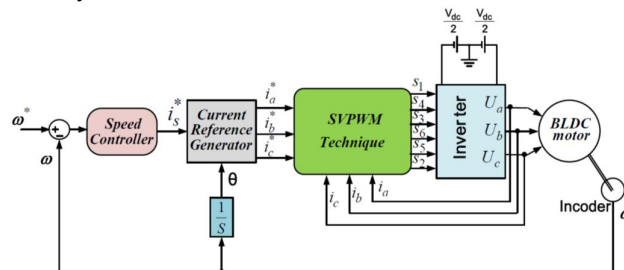

Fig.4 Block diagram of BLDC motor drive system.

As shown in the figure, the system mainly consists of four components: (1) Speed controller, here we can use one of conventional methods like PID or Sliding mode controllers. (2) Current reference controller. (3) Gates generator, two methods are used here the first is hysteresis band current PWM and the second is space vector PWM. (4) Voltage source inverter. (5) Electrical part of BLDC motor.

4. Speed Controller

The speed controller module adopts discrete sliding mode control (SMC) algorithm. The inputs of the module are ω^* and ω. ω^* is the reference signal (r/min) and ω is the feedback signal of the rotating speed. The output signal has negative saturated limiting value and positive saturated limiting value. The saturated limiting value is the maximum current value. Fig.5 is the structure of the speed control module [21].
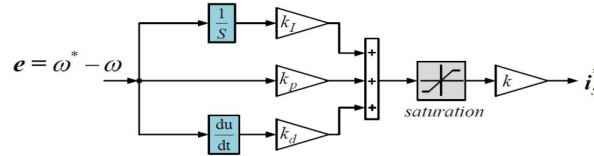

Fig.5 The structure of the speed control module

we can use the control input [21]:

$$u = u_s + u_{eq} \tag{9}$$

Where $u_s = -k.sat(s)$

First the speed error is introduced:

$$e(k) = \omega^*(k) - \omega(k)$$

Where $\omega^*(k)$ and $\omega(k)$ are the respective responses of the desired reference track and actual speed, at the k the sampling interval and $e(k)$ is the speed error. The sliding surface (s) is defined with the tracking error (e) and its integral ($\int e\,dt$) and rate of change ($\dot{e}$).

$$s = \lambda_3\,\dot{e} + \lambda_2\,e + \lambda_1 \int e\,dt \tag{10}$$

Where, λ_1, λ_2 and λ_3 are a strictly positive real constant. The basic control law of Sliding Mode Controller is given by:

$$\begin{aligned} i_s^* = u_s &= -k.sat(s) \\ &= -k.sat(\lambda_3\,\dot{e} + \lambda_2\,e + \lambda_1 \int e\,dt) \end{aligned} \tag{11}$$

Where K is a constant parameter, sat $(\cdot)$ is the saturation function and S is the switching function.

5.The reference current generating module

The reference current generating module has two inputs. One is the output of the speed control module, i_s^*, and the other is the angular displacement signal of the rotor angle. The output of the module is the current of the three-phase winding. Table 1 lists the relationship of angle (θ) and the current of the three-phase winding. We can use S-function in MATLAB for application the information in table.1 to obtain the three current references i_a^*, i_b^*, i_c^*.

Table.1 The relationship of inputs and outputs of the reference current generating module.

θ	The current of the three-phase winding		
	i_a^*	i_b^*	i_c^*
$0 \square \pi/3$	i_s^*	$-i_s^*$	0
$\pi/3 \square 2\pi/3$	i_s^*	0	$-i_s^*$
$2\pi/3 \square \pi$	0	i_s^*	$-i_s^*$
$\pi \square 4\pi/3$	$-i_s^*$	i_s^*	0
$4\pi/3 \square 5\pi/3$	$-i_s^*$	0	i_s^*
$5\pi/3 \square 2\pi$	0	$-i_s^*$	i_s^*

6. Voltage Source Inverter

Use the MOSFET three-phase bridge in SimPower System in MATLAB/Simulink as the inverter. The MOSFET in the inverter open and close in order, according to the PWM signal provided by the current controller and generate the Square wave current output. In Eq. 1 we need the phase voltages v_a, v_b, v_c , but from the bridge we can obtain the voltages v_{ao}, v_{bo} v_{co} so we calculate the neutral point to ground voltage v_{no} from

$$v_{no} = \frac{(v_{ao} + v_{bo} + v_{co} - e_a - e_b - e_c)}{3} \qquad (12)$$

Then we can calculate the phase voltages from

$$v_a = v_{ao} - v_{no}$$
$$v_b = v_{bo} - v_{no} \qquad (13)$$
$$v_c = v_{co} - v_{no}$$

Fig. 6 shows how DC power is converted into AC power. The voltage measurement works as a buffer, which can make basic units in the figure compatible with each other.
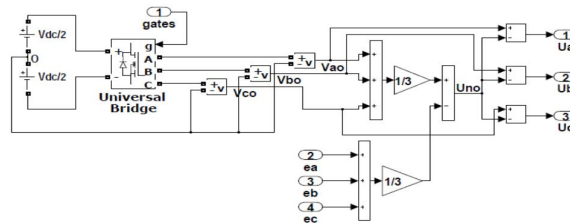

Fig.6 The structure of the voltage source Inverter.

7. Three digits SVPWM switching mode

Five steps can be identified to implement the space vector modulation technique:

   Step1. Definition of the possible switching
           vectors in output voltage space.
   Step2. Identification of the separation planes
           between the sectors in the output
           voltage space.
   Step3. Identification of the boundary planes
           in the output voltage space.
   Step4. Obtaining decomposition matrices.
   Step5. Definition of the switching sequences.

Fig. 4 shows the typical structure of a BLDC motor connected to a Voltage Source Inverter.

For this three phase power inverter, there are eight possible switching states. Six of them lead to non-zero phase voltages and the two interchangeable states lead to zero phase voltages. When mapped in a 2D-frame fixed to the stator using Concordia transformation [18], [19], the six non-zero phase voltages form the vertices of a hexagon as shown in Fig. 7.

$$\begin{bmatrix} v_\alpha \\ v_\beta \end{bmatrix} = \begin{bmatrix} 1 & -0.5 & -0.5 \\ 0 & \sqrt{3}/2 & -\sqrt{3}/2 \end{bmatrix} \times \begin{bmatrix} v_a \\ v_b \\ v_c \end{bmatrix} \qquad (14)$$
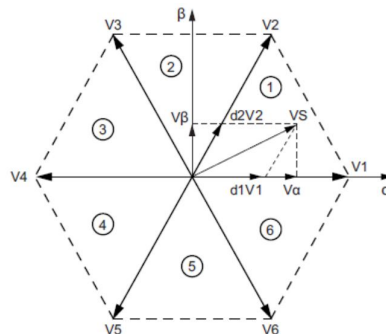

Fig.7 Eight possible switching configurations in the Concordia reference frame.
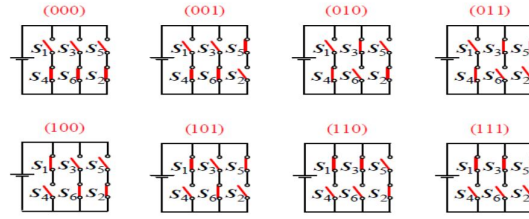
Fig.8 Possible switching configuration of a three phase inverter.

As shown in Fig. 7, the angle between two successive non-zero voltages is always 60°. In complex form, these non-zero phase voltages can be written as

$$V_k = E\, e^{j \times (k-1) \times \frac{\pi}{3}}$$ (15)

with $k = 1$ to 6 and $V_0 = V_7 = 0$ V

Table 1 shows the line-to-line and line-to-neutral voltages in each of the eight possible configurations of the inverter.

Table 1: Switching configurations and output voltages of a 3-phase inverter.

S_{a+}	S_{b+}	S_{c+}	S_i	V_{ab}	V_{bc}	V_{ca}	V_{an}	V_{bn}	V_{cn}	V_α	V_β	V_i
0	0	0	S_0	0	0	0	0	0	0	0	0	V_0
0	0	1	S_1	0	$-E$	E	$-E/3$	$-E/3$	$+2E/3$	$-E/2$	$-E\sqrt{3}/2$	V_5
0	1	0	S_2	$-E$	E	0	$-E/3$	$+2E/3$	$-E/3$	$-E/2$	$E\sqrt{3}/2$	V_3
0	1	1	S_3	$-E$	0	E	$-2E/3$	$-E/3$	$-E/3$	$-E$	0	V_4
1	0	0	S_4	E	0	$-E$	$+2E/3$	$-E/3$	$-E/3$	E	0	V_1
1	0	1	S_5	E	$-E$	0	$E/3$	$-2E/3$	$E/3$	$E/2$	$-E\sqrt{3}/2$	V_6
1	1	0	S_6	0	E	$-E$	$E/3$	$E/3$	$-2E/3$	$E/2$	$E\sqrt{3}/2$	V_2
1	1	1	S_7	0	0	0	0	0	0	0	0	V_7

In the Concordia frame shown in Fig. 7, any stator voltage $V_s = V_\alpha + jV_\beta$ $= V_{sm}\cos(\theta) + V_{sm}\sin(\theta)$ located inside this hexagon belongs to one of the six sectors and can be expressed as a linear combination of the two non-zero phase voltages which delimit this sector: $V_s = d_k V_k + d_{k+1} V_{k+1}$. Equating $d_k V_k + d_{k+1} V_{k+1}$ to $V_{sm}\cos(\theta) + V_{sm}\sin(\theta)$ in each sector leads to the expressions of the duty cycles shown in Table 2. Because the inverter cannot generate instantaneously the space vector PWM principle consists in producing a T_s-periodic voltage whose average value equals V_s, by generating V_k during $T_k = d_k T_s$ and V_{k+1} during $T_{k+1} = d_{k+1} T_s$, for every sampling period T_s. Because $d_k + d_{k+1} \leq 1$, these voltages must be completed over the switching period T_s by V_0 and/or V_7. Several solutions are possible, and the one which minimizes the total harmonic distortion (THD) of the stator current consists in applying V_0 and V_7 during the same duration

$$T_0 = T_7 = \frac{1 - d_k - d_{k+1}}{2} \times T_s$$

V_0 is also applied at the beginning and at the end of the switching period, whereas V_7 is applied at the midpoint. As an illustration, the upper side of Fig. 9 shows the waveforms obtained in sector 1.

Table 2: Expressions of the duty cycles in each sector.

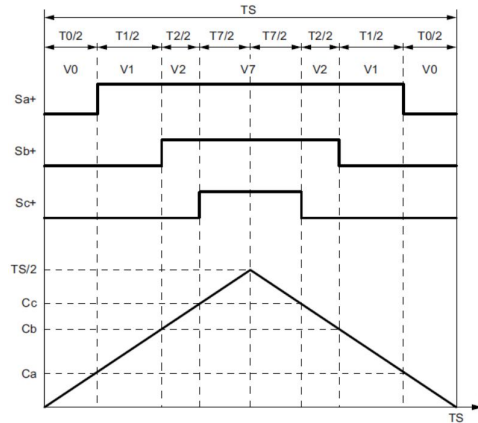| Sector Number	θ	d_k	d_{k+1}
1	$\left[0, \frac{\pi}{3}\right]$	$\frac{2}{\sqrt{3}} \times \frac{V_s}{E} \times \sin\left(\frac{\pi}{3} - \theta\right)$	$\frac{2}{\sqrt{3}} \times \frac{V_s}{E} \times \sin(\theta)$
2	$\left[\frac{\pi}{3}, \frac{2\pi}{3}\right]$	$\frac{2}{\sqrt{3}} \times \frac{V_s}{E} \times \sin\left(\frac{\pi}{3} + \theta\right)$	$\frac{2}{\sqrt{3}} \times \frac{V_s}{E} \times \sin\left(\frac{5\pi}{3} + \theta\right)$
3	$\left[\frac{2\pi}{3}, \pi\right]$	$\frac{2}{\sqrt{3}} \times \frac{V_s}{E} \times \sin(\theta)$	$\frac{2}{\sqrt{3}} \times \frac{V_s}{E} \times \sin\left(\frac{4\pi}{3} + \theta\right)$
4	$\left[\pi, \frac{4\pi}{3}\right]$	$\frac{2}{\sqrt{3}} \times \frac{V_s}{E} \times \sin\left(\frac{5\pi}{3} + \theta\right)$	$\frac{2}{\sqrt{3}} \times \frac{V_s}{E} \times \sin(2\pi - \theta)$
5	$\left[\frac{4\pi}{3}, \frac{5\pi}{3}\right]$	$\frac{2}{\sqrt{3}} \times \frac{V_s}{E} \times \sin\left(\frac{4\pi}{3} + \theta\right)$	$\frac{2}{\sqrt{3}} \times \frac{V_s}{E} \times \sin\left(\frac{\pi}{3} - \theta\right)$
6	$\left[\frac{5\pi}{3}, 2\pi\right]$	$\frac{2}{\sqrt{3}} \times \frac{V_s}{E} \times \sin(2\pi - \theta)$	$\frac{2}{\sqrt{3}} \times \frac{V_s}{E} \times \sin\left(\frac{\pi}{3} + \theta\right)$

Fig. 9 Inverter Switch Waveforms and Corresponding Compare Register Values.

Table 2 indicates that the duty cycles have different expressions in each sector. A thorough study of these expressions show that because $\sin(X) = \sin(\pi - X)$ all these duty cycles can be written in a unified way as :

$$d_k = \frac{2V_{sm}}{E\sqrt{3}}\sin(\theta'')$$

$$d_{k+1} = \frac{2V_{sm}}{E\sqrt{3}}\sin(\theta')$$

$$\text{with } \theta'' = \frac{\pi}{3} - \theta' \quad and \quad \theta' = \theta - (k-1)\frac{\pi}{3}$$

Since these expressions no longer depend on the sector number, they are denoted as d_1 and d_2 and the corresponding times as T_1 and T_2. The time functions T_A, T_B and T_C can be obtained from Table 3. Also the block diagram of SVPWM Inverter simulation is shown in Fig.10, we notice it consists of the block of calculating the time functions T_A, T_B and T_C, then these time functions are multiplied with their corresponding current errors i_{ea}, i_{eb}, and i_{ec}, respectively.

Table 3: Time functions for SVPWM technique.

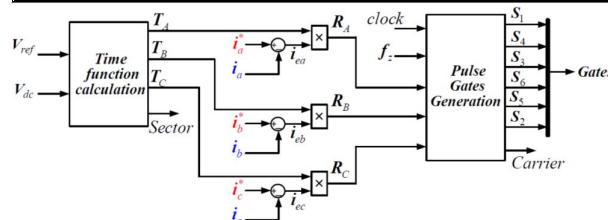| Sector No.	T_A	T_B	T_C
1	$\dfrac{T_s - T_1 - T_2}{4}$	$\dfrac{T_s + T_1 - T_2}{4}$	$\dfrac{T_s + T_1 + T_2}{4}$
2	$\dfrac{T_s - T_1 + T_2}{4}$	$\dfrac{T_s - T_1 - T_2}{4}$	$\dfrac{T_s + T_1 + T_2}{4}$
3	$\dfrac{T_s + T_1 + T_2}{4}$	$\dfrac{T_s - T_1 - T_2}{4}$	$\dfrac{T_s + T_1 - T_2}{4}$
4	$\dfrac{T_s + T_1 + T_2}{4}$	$\dfrac{T_s - T_1 + T_2}{4}$	$\dfrac{T_s - T_1 - T_2}{4}$
5	$\dfrac{T_s + T_1 - T_2}{4}$	$\dfrac{T_s + T_1 + T_2}{4}$	$\dfrac{T_s - T_1 - T_2}{4}$
6	$\dfrac{T_s - T_1 - T_2}{4}$	$\dfrac{T_s + T_1 + T_2}{4}$	$\dfrac{T_s - T_1 + T_2}{4}$

Fig. 10 View on the block of SVPWM Inverter In figure.4 using three digits switching mode.

So a new references are generated $R_A = T_A \times i_{ea}$, $R_B = T_B \times i_{eb}$, and $R_C = T_C \times i_{ec}$. These new references are compared with a triangular wave and the corresponding gate signals are obtained as shown in Fig. 11.
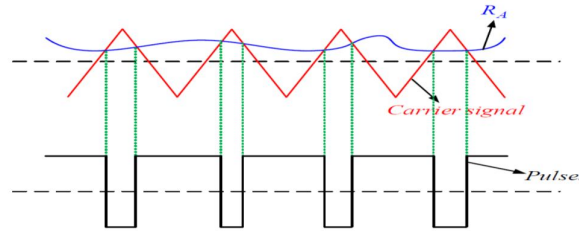

Fig. 11. Comparison of References and carrier signal (triangle waveform).

8. Six digits SVPWM switching mode

The 120° switch-on mode is adopted to reduce the torque ripple, improve the efficiency and obtains the maximum torque with the constant phase current for a three-phase trapezoidal PM BLDC motor in Y connection. Six binary digits are needed to represent the voltage space vectors in this mode. Each binary number represents a power switch's switch-on or switch-off, i.e. "1" means switch-on, while "0" means switch-off. The relationship between the conduction state of every power switch and non-zero voltage space vector corresponding is shown in Fig. 12. There is only one zero vector in 120° switch on mode, i.e. both the upper arm and lower arm are switching off at the same time.
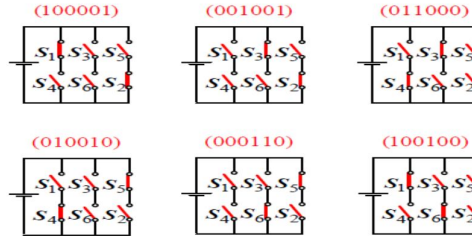

Fig. 12 Non-zero fundamental voltage space vectors in different switching states.

A-B-C axes are three-phase stator axes of the BLDC motor and the region is divided into six sectors by non-zero voltage space vectors in Fig. 13. The voltage space vector in any 60° sector can be composed of two adjacent switching state vectors and the zero vector. $\vec{U}_{out}$ rotates counterclockwise and θ is the angle between $\vec{U}_{out}$ and the α axis in the $\alpha - \beta$ frame. The amplitude of the phase voltage is $\frac{1}{2}U_d$ in 120° switch-on mode and hence the six fundamental non-zero voltage space vectors (k = 1, 2, 3, 4, 5, 6) shown in Fig. 13, can be expressed as

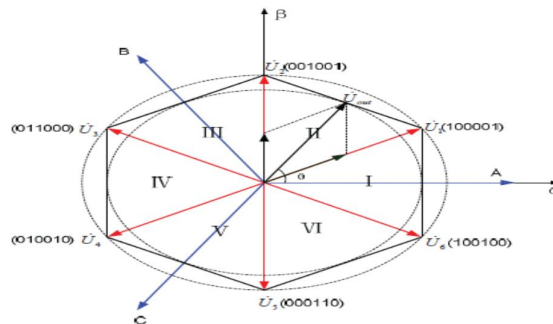$$\vec{U}_x = \frac{1}{2}U_d \, e^{j\left[\frac{\pi}{6} + (k-1) \times \frac{\pi}{3}\right]} \tag{16}$$

Fig.13 Non-zero voltage space vector in the Concordia reference frame.

For the application of the six digits switching mode we used the same model of three digits switching mode but the signals of gates ($S_1', S_2', S_3', S_4', S_5', S_6'$) is changed to the final gate pulses of

inverter ($S_1, S_2, S_3, S_4, S_5, S_6$) after returning to Fig. 12 which is related to the six digits switching mode. Thus the whole schematic of six digits SVPWM switching mode Inverter becomes as Fig.14.
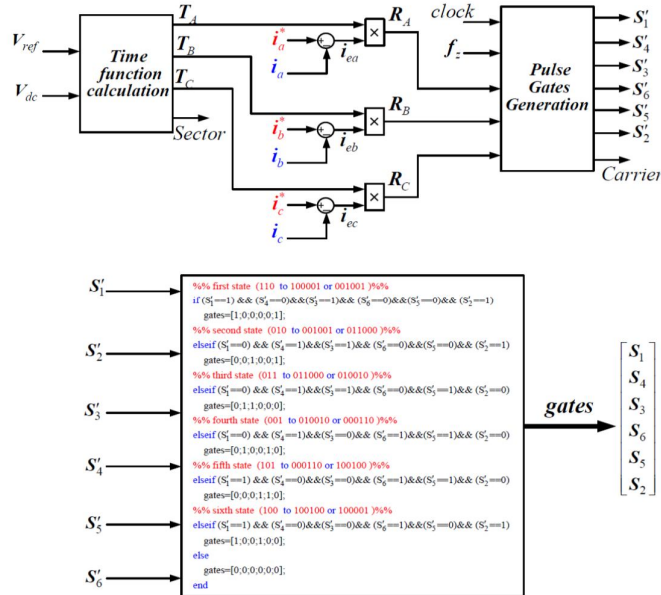

Fig. 14. View on the block of SVPWM Inverter In figure.4 using six digits switching mode.

9. SIMULATION RESULTS

In this work, the simulated module of BLDC motor drive control system using hysteresis band current PWM and SVPWM techniques is established in the environment of Simulink. The simulated parameters are set as follows in Table-4. The system is started in the load state of 0.1 [N.m]. at t=2.5s, the system is loaded 0.5 [N.m], and at t=5s, the load abruptly becomes 0.1 [N.m].

Table 4: Parameters of BLDC motor.

DC Link Voltage	$V_{dc} = 12$ [Volt]
Number of pole pairs	$P = 1$
phase resistance	$R = 0.1$ $[\Omega]$
self inductance	$L = 2$ $[mH]$
Mutual inductance	$M = 0.5$ $[mH]$
Moment of inertia	$J = 0.002$ $[kg.m^2]$
Damp coefficient	$B = 0.0002 [N.m.s.rad^{-1}]$
Rate of rotating speed	$n = 600 [rpm]$
Factor of EMFs	$k_e = 0.025$
Sliding Mode Parameters	$\lambda_2 = 10, \lambda_1 = 0.01, \lambda_3 = 0.03$
saturation bound of output	± 20
sampling period	$T_s = 0.001$ $[s]$
Frequency of carrier	$f_z = 3000$ Hz
Torque Load	$T_L = 0.1 \square 0.5$ $[N.m]$

9.1. Three digits SVPWM switching mode:

The simulated results of phase current (I_{abc}), back EMFs (E_{abc}), rotor speed (ω) and torque (T_e) waveforms for the Hysteresis Band Current PWM method are shown in Fig. 15 while more detailed views of them is depicted in Fig.16. The motor is allowed to run at 600 rpm. Also Fig.17 shows the output voltage V_{an} of inverter, and Fig.18 shows the control signals for the six switches.
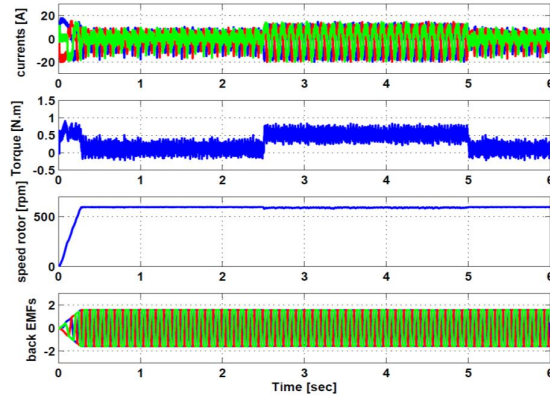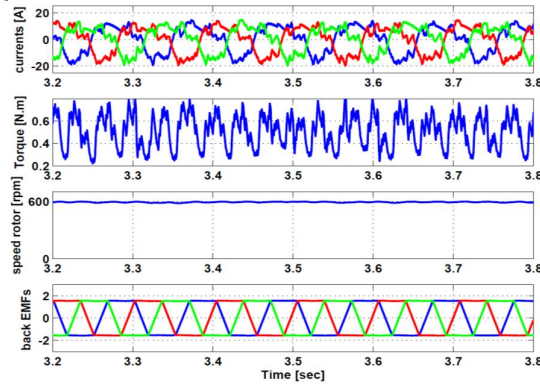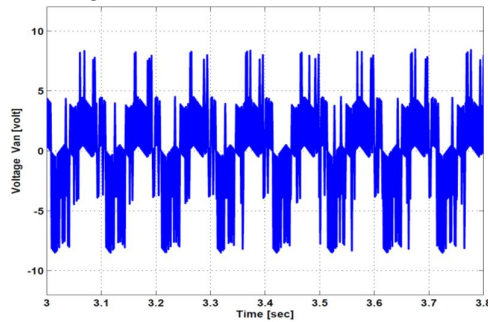
Fig. 15. Simulated results for SVPWM (three digits mode).

Fig. 16. Zoom on figure 15 from $t = 3.2$ *to* 3.8 sec.

9.2. Six digits SVPWM switching mode:

The simulated results of phase current (I_{abc}), back EMFs (E_{abc}), rotor speed (ω) and torque (T_e) waveforms for the SVPWM method are shown in Fig. 19 while their zoomed views are shown in Fig.20. The motor is allowed to run at 600 rpm. Also Fig.21 shows the output voltage V_{an} of inverter, and Fig.22 shows the control signals for the six switches.

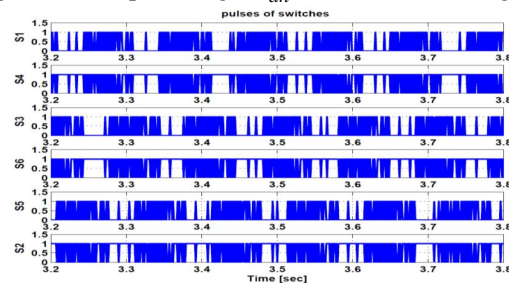Fig. 17 The output voltage V_{an} of Inverter (three digits).

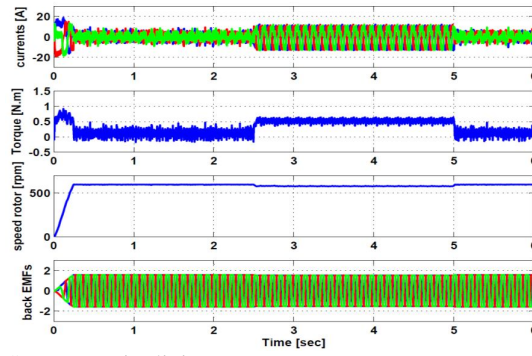Fig. 18. Pulses of switches for inverter (three digits).

Fig. 19. Simulated results for SVPWM (six digits).

As a final result from the whole figures we deduce:

- For the SVPWM method using three digits switching mode the shaft torque varies from 0.23 Nm to 0.76 Nm (in the state of torque load 0.5 Nm), so the torque ripple is 53.5% , and the phase current THD is 5%.

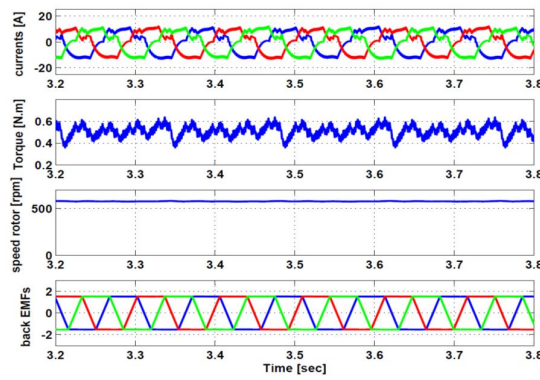For the SVPWM method using six digits switching mode the shaft torque varies

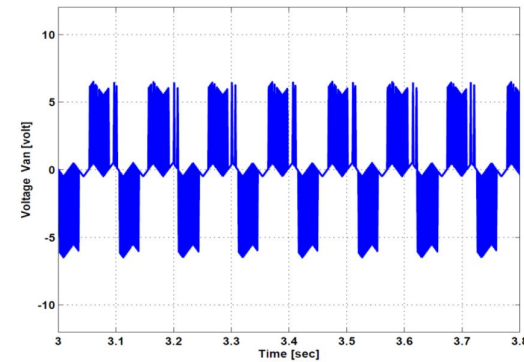Fig. 20. Zoom on figure 19 from $t = 3.2$ to 3.8 sec.

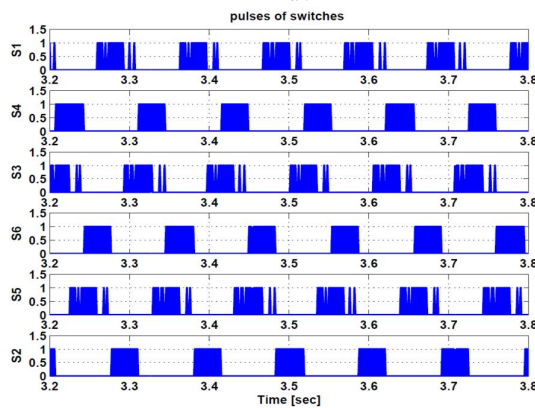Fig. 21 The output voltage V_{an} of Inverter (six digits).

Fig. 22. Pulses of switches for inverter (six digits).

- from 0.40 Nm to 0.62 Nm (in the state of torque load 0.5 Nm), so the torque ripple is 21.5%, and the phase current THD is 3%.

10. Conclusion

This paper presents the method of reducing torque ripple of the BLDC motor using new SV-PWM technique. Comparative study is carried out in which the response of three digits switching mode is compared with six digits switching mode. It is obvious from simulation results that the controller performance with six digits is much more efficient than three digits in terms of torque ripple, and current phase THD. Hence it can be concluded that six digits switching mode SVPWM Inverter provides an efficient algorithm for obtaining improved and accurate performance of a system.

REFERENCES

[1] R. Krishnan, "Electric Motor Drives Modeling, Analysis and Control", Prentice Hall, 2001.

[2] T. Miller, "Brushless PM and Reluctance Motor Drives," Oxford, UK. Clarendon, 1989.

[3] B. K. Bose, "Power Electronics and Variable Frequency Drives," IEEE Press., Piscataway, NJ., 1996.

[4] P. Vas, "Sensorless Vector and Direct Torque Control," Oxford Science Publications, New York, 1998.

[5] P. Yedamale, M. Technology, "Brushless DC (BLDC) Motor Fundamentals," DS00885A ,AN885 Manual, 2003.

[6] http://www.ecnmag.com/ article-brushless-dc-motor-control-111609, "Brushless DC Motor Control Techniques", 2009.

[7] J. R. Hendershot, T. Miller, "Design of Brushless Permanent Magnet Motors", Oxford Magna Physics:, pp. 5-1, 1994.

[8] T. M. Jahns, W. L. Soong, "Pulsating Torque Minimization Techniques for Permanent Magnet AC Motor Drives-A Review," IEEE Trans. on Ind. Elect., Vol. 43, No. 2, Apr., pp. 321-330. 1996.

[9] J. H. Song, I. Choy, "Commutation Torque Ripple Reduction in Brushless DC Motor Drives Using a Single DC Current Sensor," IEEE Trans. on Power Electr., Vol. 19, No. 2, Mar., pp. 312-319. 2004.

[10] R. Carlson, M. L. Mazenc, J. C. S. Fagundes, "Analysis of Torque Ripple due to Phase Commutation in Brushless DC Machines", IEEE Trans. Ind. Appl., Vol., 28, pp. 632-638, May.,June. 1992.

[11] T. M. Jahns, W. L. Soong, "Pulsating Torque Minimization Techniques for Permanent Magnet AC Motor Drives Review", IEEE Trans. Ind. Electron., Vol. 43, pp. 321-330, Apr. 1996.

[12] Y. Liu, Z. Q. Zhu, D. Howe, "Commutation-Torque Ripple Minimization in Direct Torque Control PM Brushless DC Drives," IEEE Trans. Vol. 43, pp. 1012-1017, Jul., Aug., 2007.

[13] J. H. Soong, I. Choy, "Commutation Torque Ripple Minimization in Brushless DC Motor Using a Single DC current Sensor," IEEE Trans., Vol. 19, no.2, pp. 312-319, Mar., 2004.

[14] Y. Sozer, D. A. Torrey, "Adaptive Torque Ripple Control of Permanent Magnet Brushless DC Motors," Proc. 13th Annual Appl. Power Elect. Conf. and Exposition, Vol. 1, 15-19 Feb. 1998, pp.86- 92.

[15] C. T. Pan, E. Fang, "A Phase Locked Loop Assisted internal Model Adjustable Speed Controller for BLDC Motors," IEEE Trans. on Indu. Elect., Vol. 55, No.9, pp. 3415-3425, 2008.

[16] Q. Wu, G. Meng, H. Xiong, H. Li, L. Zhou, "A Novel Starting Control for Sensor less Three Phase Permanent Magnet Brushless DC Motor", IEEE., 2011.

[17] C. Hong, B. Zhou, "Over Modulation Strategy of Matrix Converter Driving Brushless DC Motor Systems", IEEE., 2009.

[18] ATMEL, "BLDC/BLAC Motor Control Using a Sinus Modulated PWM Algorithm with Atmel ATmega32M1", Appl. Note, Atmel Corporation. 2012.

[19] V. Viswanathan, S. Jeevananthan, "A Novel Current Controlled Space Vector Modulation Based Control Scheme for Reducing Torque Ripple in Brushless DC Drives", Inter. Journal of Computer Applications (0975 – 8887) Vol. 28– No.2, Aug., 2011.

[20] M. R. Feyzi, M. Ebadpour, S. A. K. M. Niapour, A. Feizi, R. M. Aghdam "A New Single Current Strategy for High Performance Brushless DC Motor Drives", CCECE 2011, Niagara, Canada, IEEE CCECE, 2011.

[21] M. Fallahi, S. Azadi, "Adaptive Control of a DC Motor Using Neural Network Sliding Mode Control", Proceed. of the Inter. Multi Conf. of Eng. and Computer Scientists Mar. 18 – 20, Hong Kong. 2009